NONLINEAR GROUND VIBRATION IDENTIFICATION OF AN F-16 AIRCRAFT - PART II: UNDERSTANDING NONLINEAR BEHAVIOUR IN AEROSPACE STRUCTURES USING SINE-SWEEP TESTING

T. Dossogne[1], J.P. Noël[1], C. Grappasonni[1], G. Kerschen[1], B. Peeters[2], J. Debille[2], M. Vaes[3], J. Schoukens[3]

[1] Space Structures and Systems Lab
Aerospace and Mechanical Engineering Department
University of Liège, Liège, Belgium
tdossogne, jp.noel, chiara.grappasonni, g.kerschen@ulg.ac.be

[2] Siemens Industry Software
Leuven, Belgium
bart.peeters, jan.debille@siemens.com

[3] ELEC Department
Vrije Universiteit Brussels, Belgium
mark.vaes, johan.schoukens@vub.ac.be

Keywords: Ground Vibration Testing, F-16 aircraft, structural nonlinearities, sine-sweep excitation.

Abstract: Although they are generally modelled as linear systems, aircraft structures are known to be prone to nonlinear phenomena. A specific challenge encountered with fighter aircraft, besides aeroelastic nonlinearity, is the modelling of the wing-to-payload mounting interfaces. For large amplitudes of vibration, friction and gaps may be triggered in these connections and markedly impact the dynamic behaviour of the complete structure. In this series of two papers, the nonlinear dynamics of an F-16 aircraft is investigated using rigorous methods applied to real data collected during a ground vibration test campaign.

The present work focuses on the analysis of sine-sweep measurements in order to get an insightful understanding about the nonlinear behaviour of the aircraft. To this extent, restoring force surface and wavelet transform methods are applied both on the collected GVT data and simulation results performed on a simple numerical model of the F-16 wing and its payload.

1 INTRODUCTION

There exists in industry an ever-increasing pressure to reduce the cost and development cycles while meeting strict technological and environmental objectives. A compelling illustration of this statement comes from the aerospace sector, where Europe's 2020 vision aims at a 50 % cut in CO_2 emissions per passenger kilometre, which means a 50 % cut in fuel consumption [1]. This results in the design of continuously lighter aircraft structures, which are inevitably prone to severe nonlinear vibration problems due to their greater flexibility [2]. Currently, this not only limits the aircraft flight envelopes, but also implies decreased fatigue lifespans for airframes and decreased comfort conditions for passengers.

It is therefore not surprising to notice a growing demand in high-tech industry for a new generation of advanced structural dynamics capabilities which can accommodate the complex nonlinear reality of new products. The practicing engineers, who were used to ignore or avoid nonlinear effects during the design process, are now seeking to rigorously account for them [3]. In particular, they are looking for a methodology viable in an industrial context to detect and understand nonlinear behaviours.

Arguably one of the most popular tools to detect nonlinearity in test data is the comparison of frequency response functions (FRFs) acquired at different forcing amplitudes.

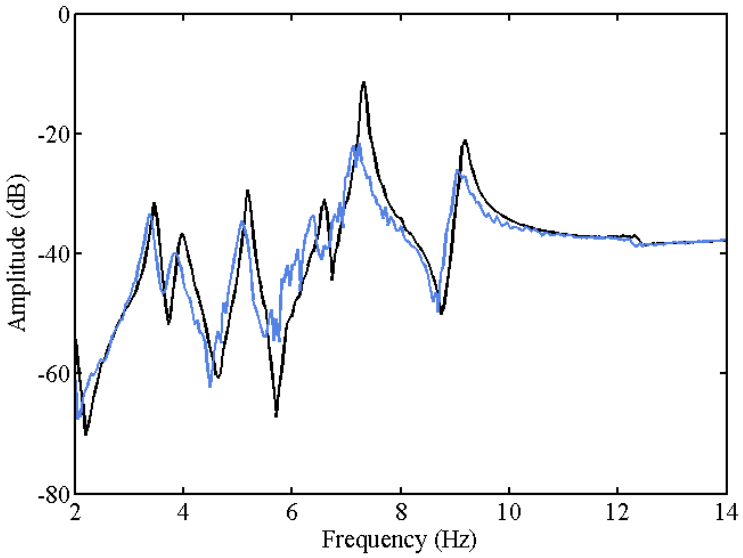

Figure 1: FRF measured at the right wing tip of an F-16 aircraft using random data.
Black curve: 12 N RMS; blue curve: 97 N RMS

A linear system obeys the homogeneity principle, which requires FRFs to be independent of the input spectrum [4]. The superposition of FRF plots, which is possible with virtually all modern spectrum analysers, is thus a reliable indicator of the activation of nonlinear behaviour in specific frequency intervals. Figure 1 represents two FRFs calculated using random data at the right wing tip of an F-16 aircraft (see Section 3 for more details about the test campaign). The black and blue curves correspond to the aircraft response at low and high excitation amplitudes, *i.e.* 12 and 97 N root-mean-squared (RMS) amplitudes, respectively. Significant nonlinear distortions are easily noticed at high level. In particular, all resonances are seen to shift toward lower frequencies. Damping is also found to increase with the input level. However, the homogeneity test does not convey any more information regarding the nature of the nonlinearity sources.

The objective of the present paper is to highlight that the analysis of sine-sweep measurements may lead to a profound understanding of the nonlinear mechanisms involved. This, in turn, may help the practicing engineer to develop a reliable model of the nonlinear structure under test. The analysis is achieved using two conceptually simple tools, namely the restoring force surface and the wavelet transform methods. Both approaches are briefly described in Section 2. They are demonstrated numerically using an aircraft wing model with a stiffness nonlinearity in Section 4. Finally, Section 5 analyses real data measured on a full-scale F-16 fighter, and reveals that the aircraft dynamics is affected by clearance nonlinearities and Coulomb friction.

2 THE RESTORING FORCE SURFACE AND WAVELET TRANSFORM METHODS

2.1 Restoring force surface plots

The restoring force surface (RFS) method, first introduced by Masri and Caughey [5] and covered in detail in the textbook [4], serves commonly as a parameter estimation technique [6-8]. This section introduces an unconventional use of the RFS method for nonlinearity characterization purposes, relying exclusively on measured signals. The starting point is Newton's second law of dynamics written for a specific degree of freedom (DOF) located next to a nonlinear structural component, namely

$$\sum_{n=1}^{n_p} m_{i,n}\ddot{q}_n + g_i(\mathbf{q},\dot{\mathbf{q}}) = p_i \tag{1}$$

where i is the DOF of interest, n_p the number of DOFs in the system, m_{ij} the mass matrix elements, $\mathbf{q}$, $\dot{\mathbf{q}}$ and $\ddot{\mathbf{q}}$ the displacement, velocity and acceleration vectors, respectively, $\mathbf{g}$ the restoring force vector encompassing elastic and dissipative effects, and $\mathbf{p}$ the external force vector. The key idea of the approach is to discard in Eq. (1) all the inertia and restoring force contributions that are not related to the nonlinear component, as they are generally either unknown, *e.g.*, the coupling inertia coefficients, or not measured, *e.g.*, the rotational DOFs. If we denote by j another measured DOF located across the nonlinear connection, Eq. (1) is therefore approximated by

$$m_{i,i}\ddot{q}_i + g_i(q_i - q_j, \dot{q}_i - \dot{q}_j) \approx p_i \tag{2}$$

If no force is applied to DOF i, a simple rearrangement leads to

$$g_i(q_i - q_j, \dot{q}_i - \dot{q}_j) \approx -m_{i,i}\ddot{q}_i \tag{3}$$

Eq. (3) shows that the restoring force in the nonlinear connection is approximately proportional to the acceleration at DOF i. Hence, by simply representing the acceleration signal, with a negative sign, measured at one side of the nonlinear connection as a function of the relative displacement and velocity across this connection, the nonlinearities can be conveniently visualized, and an adequate mathematical model for their description can then be selected.

2.2 Time-frequency analysis using the wavelet transform

The Fourier transform, which is the one-to-one transformation from a time-domain history *x(t)* to a frequency-domain spectrum $X(\omega)$

$$X(\omega) = \int_{-\infty}^{\infty} x(t)e^{-j\omega t}dt \tag{4}$$

fails to capture nonstationary effects. In this regard, the wavelet transform is an appealing alternative as it maps a time history to a time-frequency representation. It also allows adjustable time and frequency resolutions via a windowing strategy with variable-sized regions, hence outperforming the short-time Fourier transform. This makes the wavelet transform one of the most suitable techniques for analysing harmonics generated by nonlinear system in response to sine-sweep excitations [9].

The wavelet transform writes

$$X(a,b) = \frac{1}{\sqrt{a}} \int_{-\infty}^{\infty} x(t) \psi \left(\frac{t-b}{a} \right) dt \tag{5}$$

where ψ is referred to as the mother wavelet. Parameter *b* locates the observation window in the time domain, and *a* contracts or expands the window depending upon the frequency components of *x(t)*. The *Morlet* mother wavelet, which is a Gaussian-windowed complex exponential, is exploited herein for its versatility.

3 GVT SETUP AND NUMERICAL MODEL DESCRIPTION

This present study focuses on the analysis of the dynamics of an F-16 aircraft based on both experimental and numerical results, respectively from GVT measurements on the full-scale aircraft structure and simulations on a finite-element model of the wing. Those two test cases are described in the current section.

3.1 F-16 Instrumentation and Linear Modal Analysis

The GVT campaign took place on the occasion of the *Siemens LMS Ground Vibration Testing Master Class* [10] held in September 2014 at the Saffraanberg military basis in Sint-Truiden, Belgium (Figure 2 (a)). The measurements were made on a full-scale F-16 fighter equipped with two dummy payloads, mounted at wing tips (Figure 2 (b)). The aircraft was standing on its landing gears whose tyres were lightly flattened to reproduce free-free conditions [11] and the whole structure was excited through two vertical shakers, attached underneath the two wings considering a misalignment to trigger the wing torsion modes (Figure 2 (c)).

The aircraft was extensively instrumented by means of uniaxial and triaxial accelerometers, totalizing 145 measured degrees of freedom. A particular attention was given to parts of the aircraft known as potential sources of nonlinearity, namely wing-to-payload connections [12]. In such interfaces, triaxial sensors were positioned on both sides of the connection (Figure 2 (d) and (e)).

Before getting insight of the nonlinear dynamics, a linear modal analysis based on FRF's obtained for a low-level random test is performed using PolyMAX method [13]. The applied random excitation has an RMS value of 10N and covers a frequency bandwidth from 2 to 14Hz. This analysis enables the identification of two rigid-body-modes located below 4Hz and several deformation modes. Modal shapes of the four first ones are illustrated in Figure 3. Their natural frequencies and damping ratios are listed in Table 1.

(a)

(b)

(c)

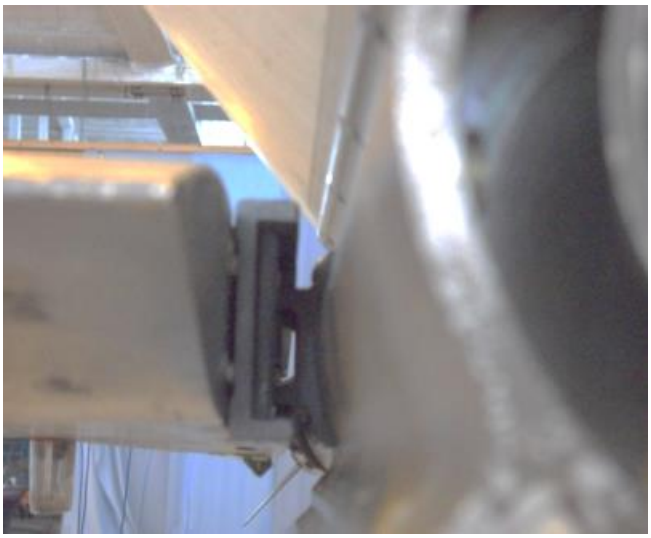

(d)

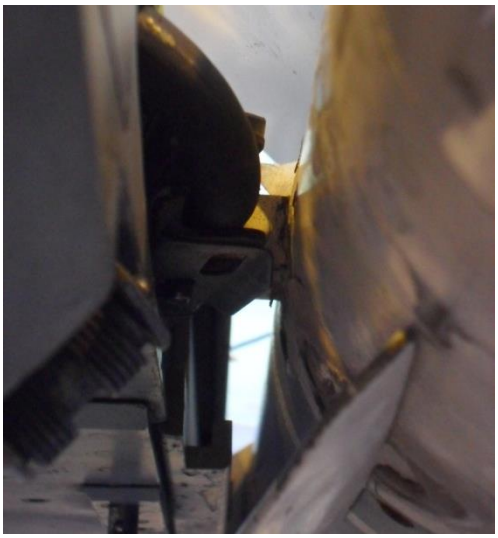

(e)

Figure 2: Ground Vibration Testing setup. (a) Instrumented F-16 aircraft; (b) dummy payload mounted on the right wing tip; (c) shaker attached underneath the right wing; (d) back connection of the mounting interface; (e) front connection of the mounting interface

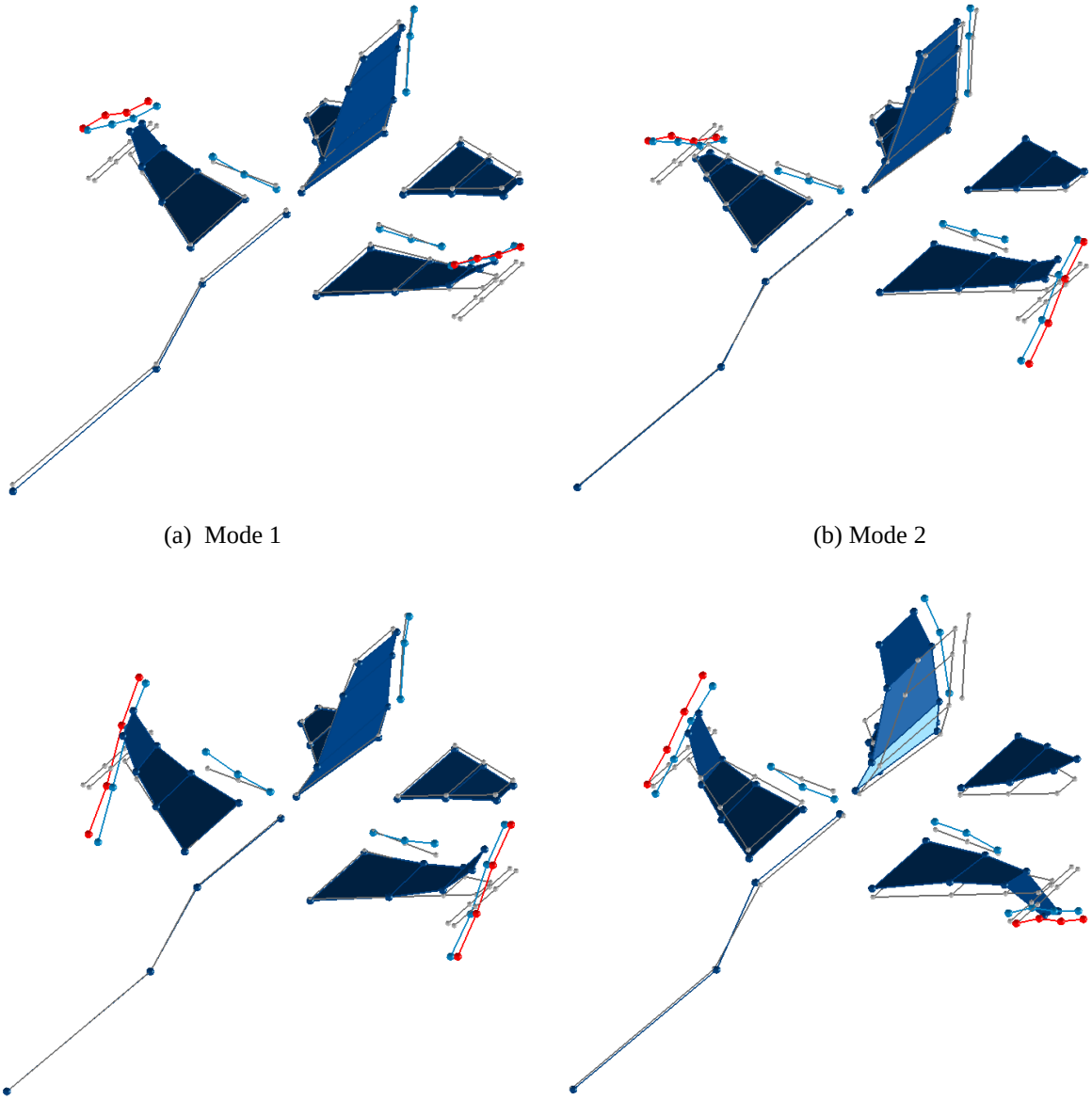

(a) Mode 1 (b) Mode 2

(c) Mode 3 (d) Mode 4

Figure 3: Deformed shapes of the flexible modes up to 10Hz estimated using the PolyMAX method

Mode	Description	Natural Frequency [Hz]	Damping Ratio [%]
1	First wing bending	5.16	0.84
2	Antisymmetric payload rotation	6.61	0.77
3	First wing torsion	7.31	0.43
4	Antisymmetric wing bending	9.14	0.74

Table 1: Frequencies and damping ratios of the flexible modes up to 10Hz estimated using the PolyMAX method

3.2 Finite Element Model Construction

A simple finite-element model of the aircraft wing and its connected payload is built with the Siemens PLM Software-LMS Samcef, in order to perform numerical experiments. The model consists of shell elements and 3D linear springs to reproduce the wing-to-payload connection (Figure 4). The different physical parameters are set such as the model exhibits same specifically chosen modes as the real F-16 aircraft, in terms of natural frequencies and modal shapes. Mainly, the model is calibrated to be able to reproduce the first wing bending mode (Mode 1) and the wing torsion mode (Mode 3) as they are the most sensitive to nonlinear phenomena (see Section 5). Regarding boundary conditions, nodes at the wing's root are clamped.

Proportional damping ($C = \alpha K + \beta M$) is also added to the structure and the values of the α and β parameters are tuned such that accelerations of similar order of magnitude as in experimental measurements are reached under the same force level. For this study case, $\alpha = 5.01\ 10^{-5}$ and $\beta = 0.52$. This leads to a damping ratio of 0.7% for the torsion mode, which is a perfectly acceptable value although a little higher than the experimental one.

The structure is then condensed using a Craig-Bampton model order reduction method in order to decrease the computational time of simulations. The model is so reduced into a linear super element containing 3 retained nodes and 10 internal modes of vibration. The 3 retained nodes are the two nodes on either side of the wing-to-payload back connection and one node on the wing, corresponding to the excitation point where the shaker is supposed to be attached.

In order to assess the accuracy of the created super element, a comparison between the modal parameters of the full and the reduced model is made based on the computation of natural frequency error and modal assurance criterion. As illustrated in Figure 5, the use of 10 internal modes is sufficient to ensure, up to 100Hz, an error on the natural frequencies below 1% and a MAC almost equal to 1 (corresponding to a perfect mode shapes correspondence).

Eventually, as the reduced-order model is still linear, a nonlinear behaviour must be introduced a posteriori by the mean of a nonlinear vertical spring localized between the two retained nodes at the back connection. This spring has a piecewise-linear behaviour (Figure 4) whose properties (e.g. clearances and stiffness's) are set to encounter the same stiffness curves as observed experimentally (see Section 5). Concretely, the discontinuities are reached at $4.8\ 10^{-5}m$ and $5.2\ 10^{-4}m$ for positive relative displacements and at $-4.8\ 10^{-5}m$ and $-4.2\ 10^{-4}m$ for negative ones.

Furthermore, as the strong discontinuities between the different linear parts of the stiffness curve can lead to convergence issues during time integration, a regularization process is imposed in those areas. There, linear branches are hence replaced by third-order Hermit interpolation polynomials to enforce the continuity of the first derivative.

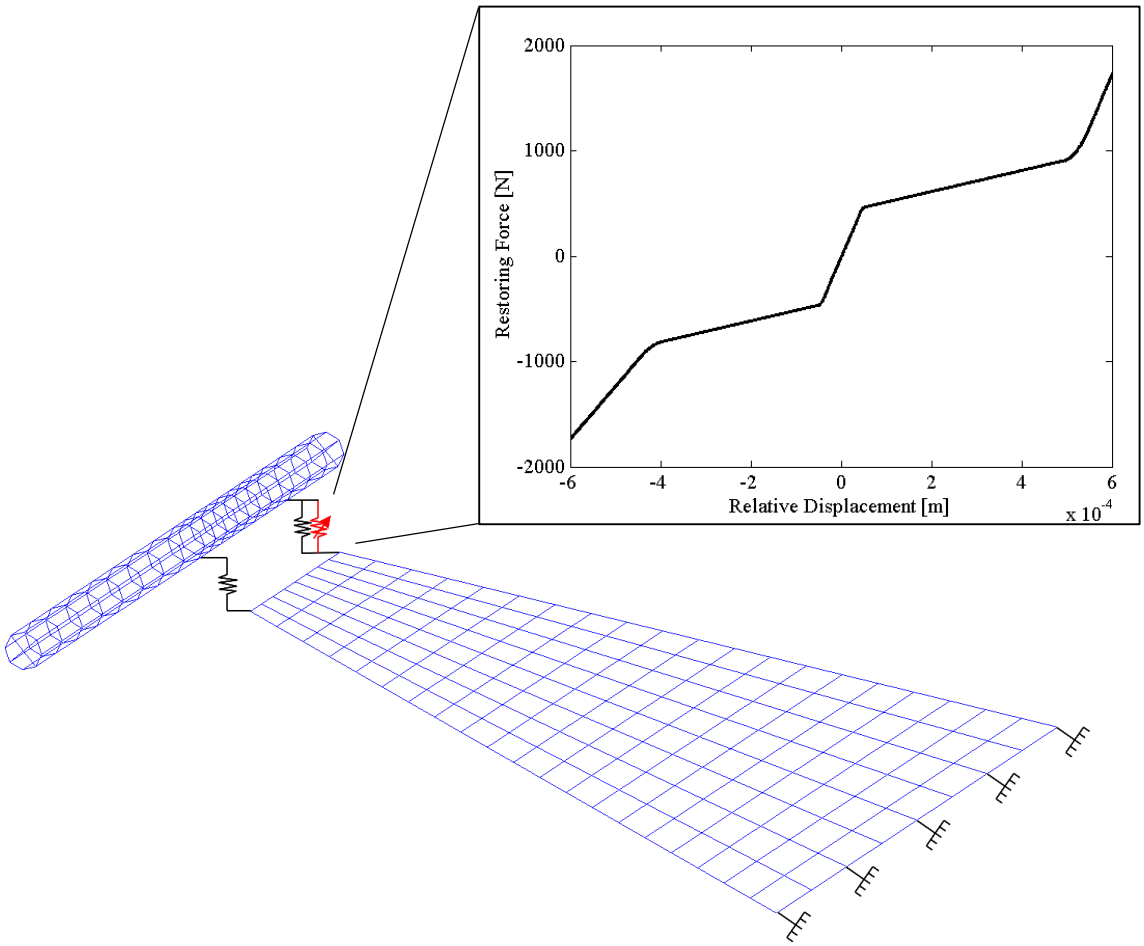

Figure 4: Finite Element model of the aircraft wing and its connected payload and stiffness curve of the back connection. Black springs: Linear springs; Red spring: Piecewise-linear spring.

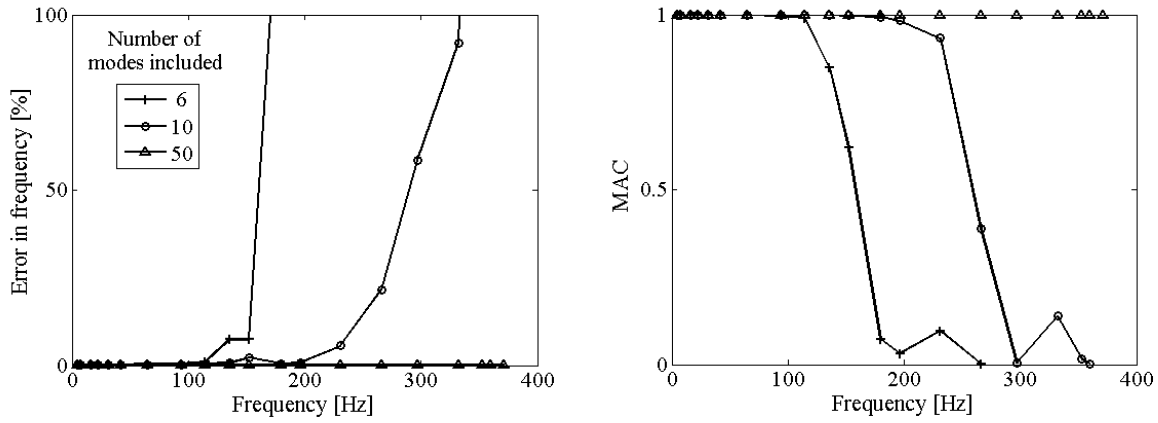

(a) (b)

Figure 5: Assessment of the accuracy of reduced-order models of the aircraft wing depending on the number of modes included in the super element. (a) Deviations in natural frequencies; (b) deviations between mode shapes quantified using the modal assurance criterion (MAC).

4 DEMONSTRATION USING A SIMPLE NUMERICAL AIRCRAFT WING MODEL

This section addresses the demonstration of the restoring force surface and the wavelet transform method on a numerical aircraft wing model described previously. The analysis will be focused on the behaviour of the back wing-to-payload connection where the nonlinear spring is acting.

As performed experimentally during the GVT measurements, a sine-sweep excitation is applied vertically under the wing (at the third retained node of the super element). This swept sine goes down at a rate of 1Hz/min, from 8 to 6Hz as only the third mode around 7Hz will be studied in this section. Indeed, this vibration mode tends to be the most prone to nonlinearities as it triggers large amplitude oscillations at the back connection. The observation of the FRF measured for both low and high levels at the connection (Figure 1) also confirms this trend as the resonance peak of the third mode experiences the biggest variation in amplitude and frequency.

The choice of a down direction for the sweep lies in the presence of a softening effect that can be observed on overlaid frequency response functions (Figure 1). Such kind of nonlinear behaviour is indeed more sensitive to downward swept-sine excitation. Different levels of excitation between 10 and 100N are considered and simulations are performed with the use of a nonlinear Newmark time integration algorithm.

Based on the obtained time series, the restoring force surface can be computed for the vertical degree of freedom localized on the wing side of the nonlinear connection. Figure 6 shows stiffness curves (cross-sections of the restoring force surface at the vicinity of zero relative velocity) for excitations of 10, 45, 70 and 100N. At low level (a), a purely linear behaviour is observed as expected, since the relative displacement has not reached the value of the first imposed discontinuity. Under an excitation of 45N, the amplitude of the oscillations becomes sufficiently high to enter into the second linear regime and the stiffness curve experiences an abrupt drop in slope (b). As the level keep increasing, the relative displacement in the connection ends reaching the second discontinuities, instigating a sudden rise in slope (d). One can also notice the outbreak of additional branches around small relative displacements (c). The causes of such disturbances are discussed later in this section.

As the complete mass, damping and stiffness matrices are known, the exact restoring force can be computed using Equation (1) without any approximation. This leads to a quantitative stiffness curve that is illustrated in Figure 7 (left) and compared with the originally implemented stiffness of the nonlinear spring (see Figure 4). Figure 7 (right) shows the same comparison but regarding the qualitative stiffness curve obtained with Equation (3). The perfect match in the left plot simply expresses that the nonlinear Newark time integration algorithm has worked properly. Nevertheless, concerning the right plot, the excellent correspondence between the qualitative curve and the rescaled implemented stiffness demonstrates the usefulness and the reliability of such qualitative approach. Although the exact stiffness coefficients cannot be estimated with such a method, the identification of the overall nonlinear behaviour in the connection and the values for the different clearances is performed efficiently.

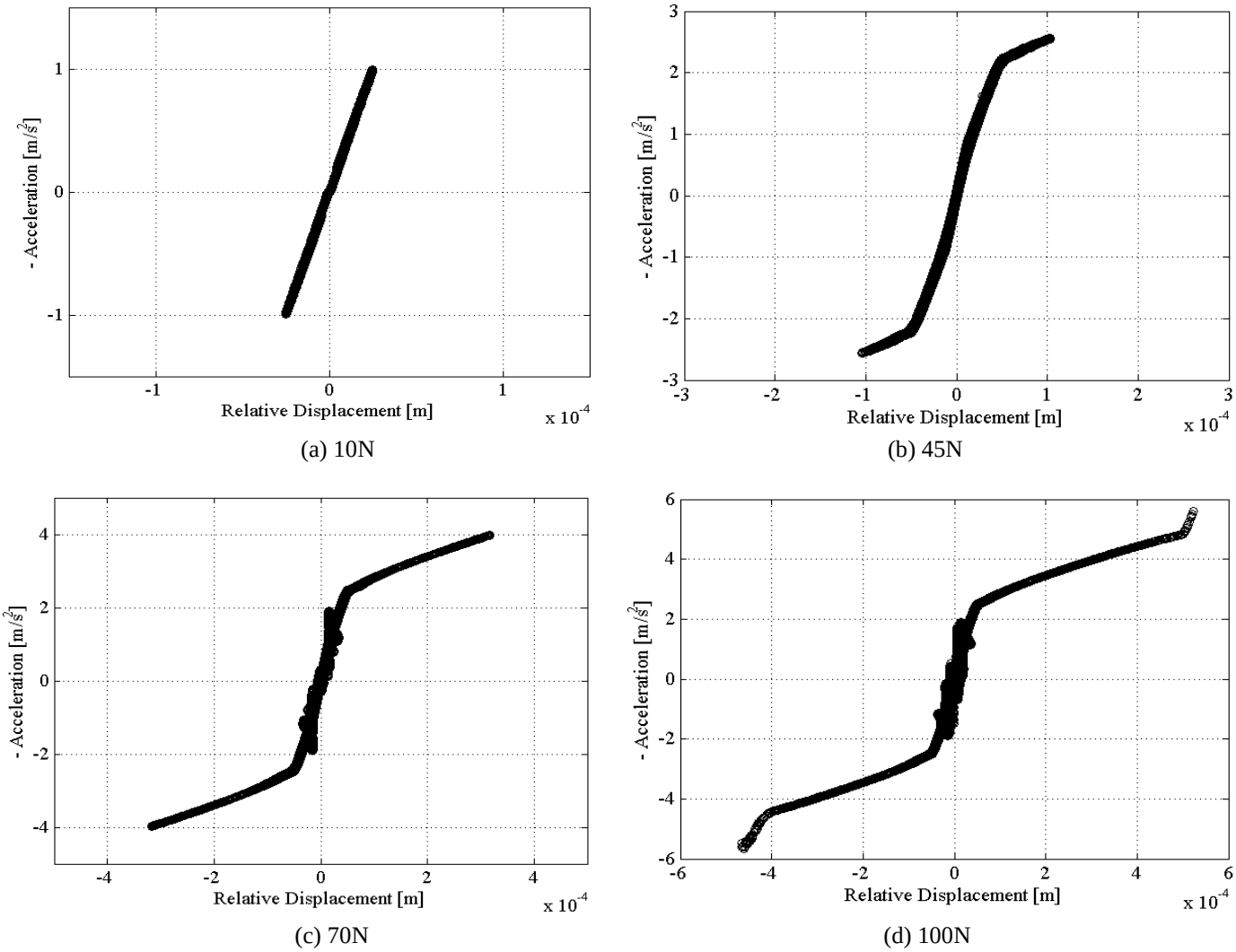

(a) 10N (b) 45N

(c) 70N (d) 100N

Figure 6: Qualitative stiffness curves across the back wing-to-payload connection around the third mode computed using RFS method for 4 different excitation levels

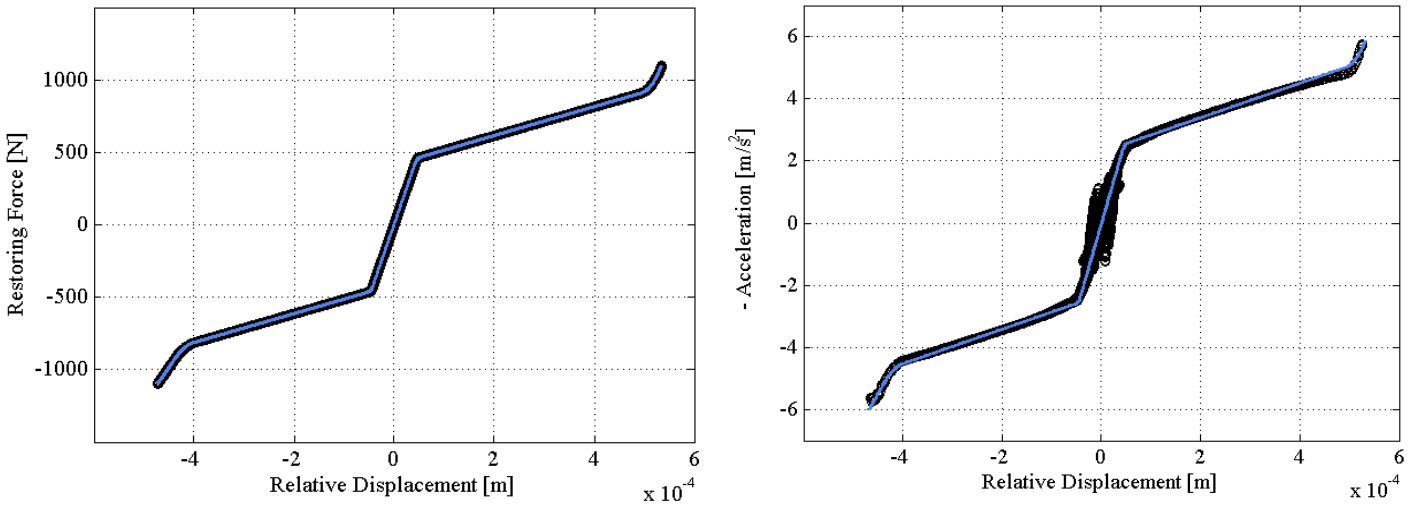

Figure 7: Quantitative (left) and qualitative (right) stiffness curves across the back wing-to-payload connection. Black dots: stiffness curves from RFS; blue lines: implemented stiffness curve in the nonlinear spring.

Figure 8 exhibits the wavelet transform amplitudes computed at the wing-sided node of the back connection for the same four excitation levels. At first, only the fundamental can be seen

(a) whereas harmonics appear in the frequency content of the acceleration under a 45N sine sweep excitation (b). Only odd harmonics pop up as the nonlinear behaviour is still symmetric at that level (see Figure 7 (b)). When the second discontinuities are reached, the nonlinearity is no longer symmetric with respect to the origin (see Figure 7 (d)) as the positive and negative clearances differ. Therefore, even harmonics also break out in the structure's response (d).

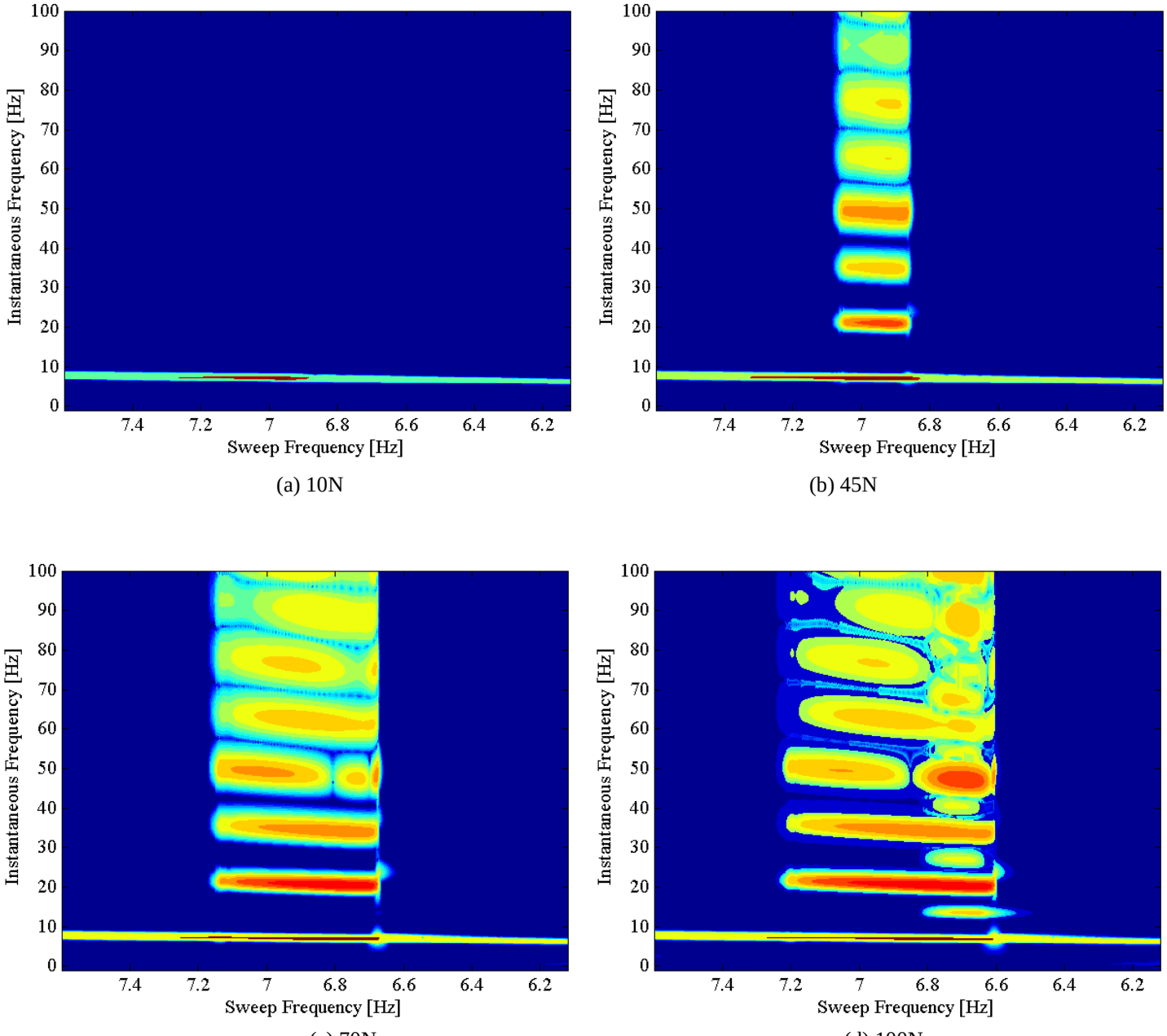

(a) 10N (b) 45N

(c) 70N (d) 100N

Figure 8: Wavelet transform amplitudes (in logarithmic scaling) of the vertical acceleration at the back wing-to-payload connection, wing side under four different levels of sine-sweep excitation

Furthermore, it can be seen that some harmonics are significantly stronger than the others and those amplitude peaks are generally localized around particular frequencies. A closer look to the wavelet transform amplitude at high level is illustrated in Figure 9 with overlaid horizontal

lines corresponding to the natural frequencies of all the actual vibration modes of the system. It is then obvious that the significant amplitudes of some harmonics correspond to existing modes at those frequencies. There exists hence a modal interaction between the wing torsion mode around 7Hz and higher order modes excited through the generation of harmonic components. For instance, the seventh harmonics increases severely as it encounters first a mode at 49Hz (7 x 7Hz) and another at 46Hz (7 x 6.6Hz). This complex nonlinear mechanism is also to be related to the emergence of additional branches in the RFS (see Figure 7 (c)). In case of modal interactions, more than one mode is contributing to the system's response. Consequently, as the RFS must be computed by assumption on a unique mode, the presence of such internal resonances can affect the quality of your stiffness curve.

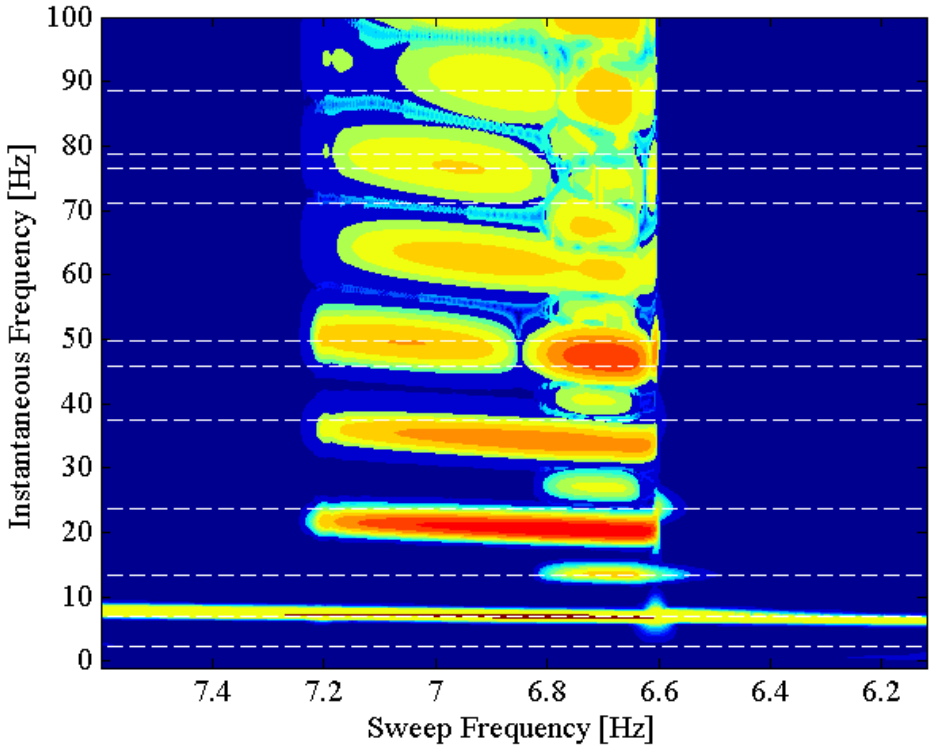

Figure 9: Wavelet transform amplitudes (in logarithmic scaling) of the vertical acceleration at the back wing-to-payload connection, wing side under a 100N sine-sweep excitation. Dashed white lines: natural frequencies of the system's vibration modes

5 EXPERIMENTAL ANALYSIS OF A FULL-SCALE F-16 AIRCRAFT

The objective of this section is to provide an insightful understanding of the nonlinear mechanisms involved in the F-16 dynamics by exploiting real GVT data obtained with sine-sweep measurements. The applied excitation is then a decreasing and linear swept sine from 15 to 2Hz and several force amplitudes are considered. For the sake of conciseness, the current analysis is restricted to the third mode as such a mode is the most prone to trigger nonlinear mechanisms, as explained in the previous section. This trend will be clearly confirmed later during the analysis of the wavelet transforms over the whole excited frequency band. Times series of the acceleration measured under a 95.6N sine sweep is shown in Figure 10, where the considered sensor is located on the payload side of the back wing-to-payload connection (see Figure 2 (d)). The blue region depicts the portion of the signal around the third mode considered for the computation of restoring force surfaces.

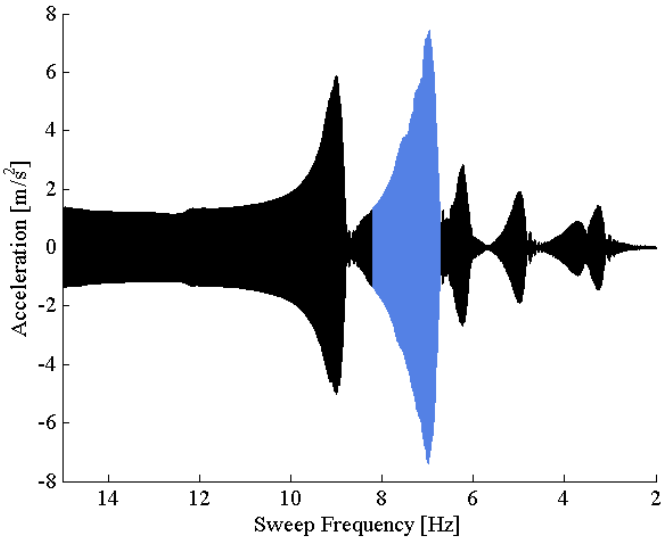

Figure 10: Time series of vertical acceleration measured at the back connection (payload side) under a 95.6N sine sweep excitation

Restoring force surfaces are computed based on measurements from 6 different levels of excitation. Cross-sections at the vicinity of zero relative velocity and zero relative displacement give, respectively the stiffness and damping curves that are represented in Figure 11 (a)-(l). For a small excitation level of 9.6N, the stiffness curve (a) remains linear whereas a small loop in the damping curve indicates the presence of hysteresis phenomenon. Sudden decreases in the slope of the stiffness curve at 28.8N (c) express a discontinuous softening behaviour that remains for higher levels (e), (g) and (i). This can be confidently attributed to the opening of the connection holding the payload. Regarding the damping curve, for increasing levels of excitation, it starts to grow smoothly (d) before suddenly reaching a plateau where the force becomes independent of the relative velocity (f), (h). Such behaviour reveals clearly the presence of Coulomb friction between the two parts of the mounting interface. The friction phenomenon becomes then asymmetric (j), (l) as the slope gets higher for positive relative velocities, tending more toward viscous damping effects. At the highest level of excitation, 95.6N, oscillations amplitude is sufficiently large to hit the boundaries of the mounting interface. This triggers strong impacts that can be observed on the stiffness curve (k) where abrupt increases in the slope appear at the extreme values. An estimation of the clearances can also be confidently performed (see Section 4). Values of 0.52mm and 0.42mm are found respectively for positive and negative relative displacements.

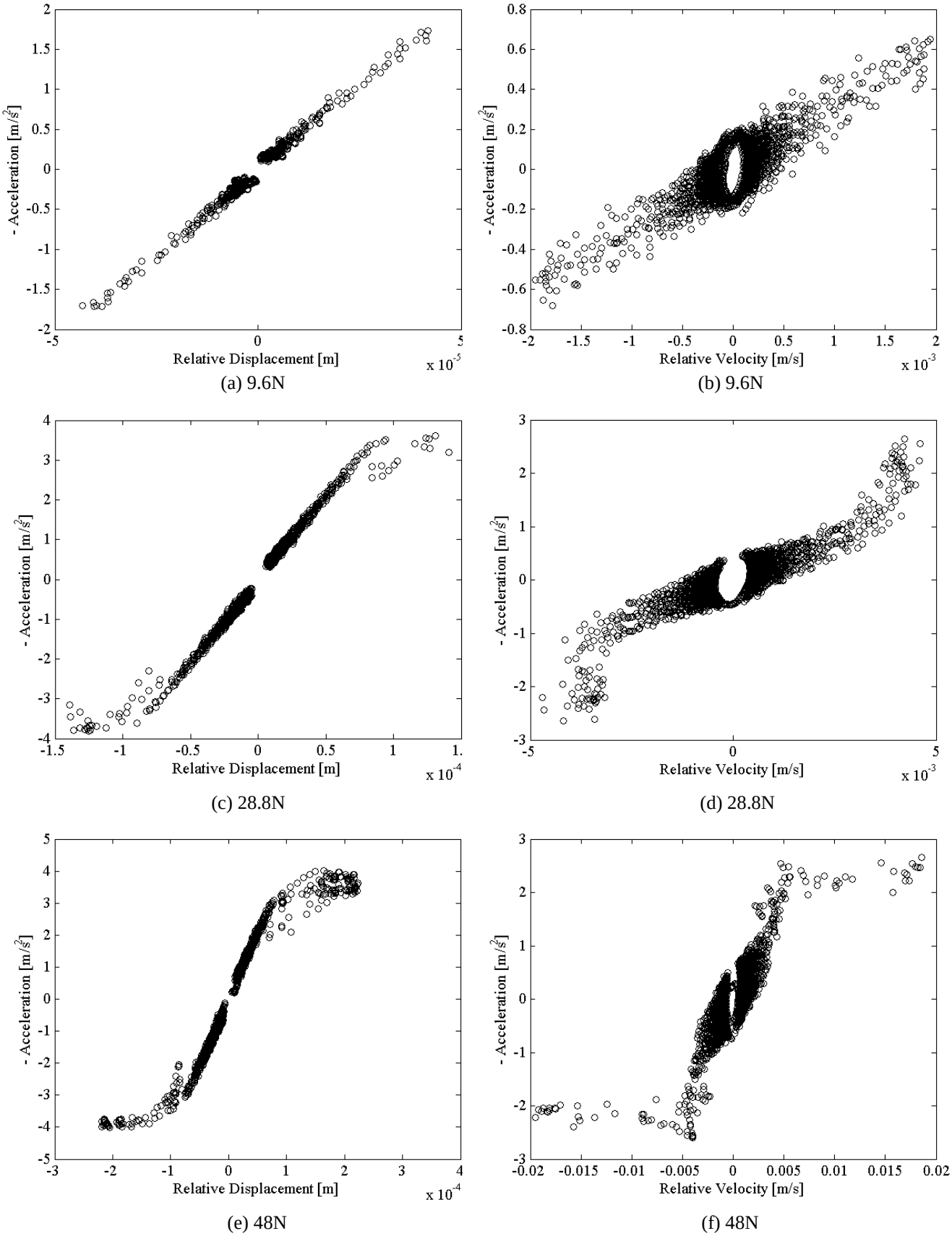

Figure 11: Qualitative stiffness (left) and damping (right) curves across the back wing-to-payload connection around the third mode computed using RFS method for 6 different levels of sine-sweep excitation

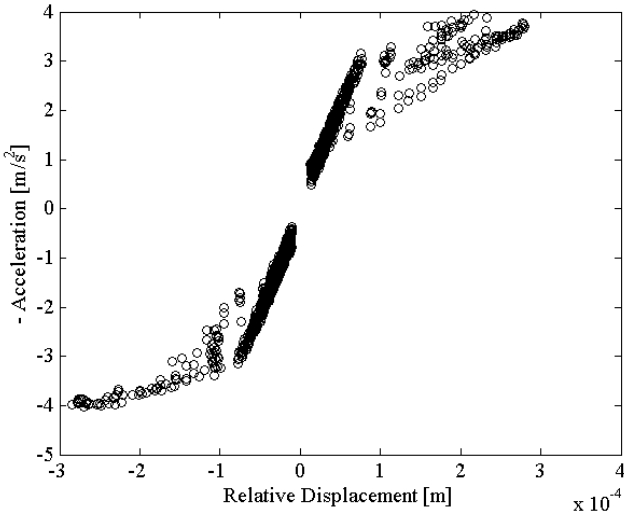

(g) 57.6N

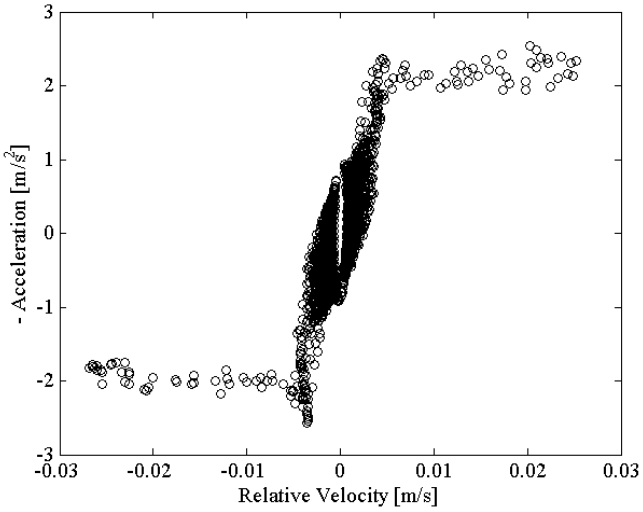

(h) 57.6N

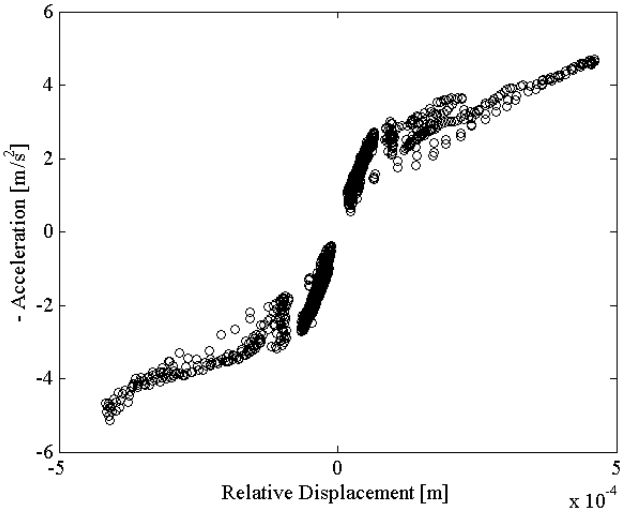

(i) 76.6N

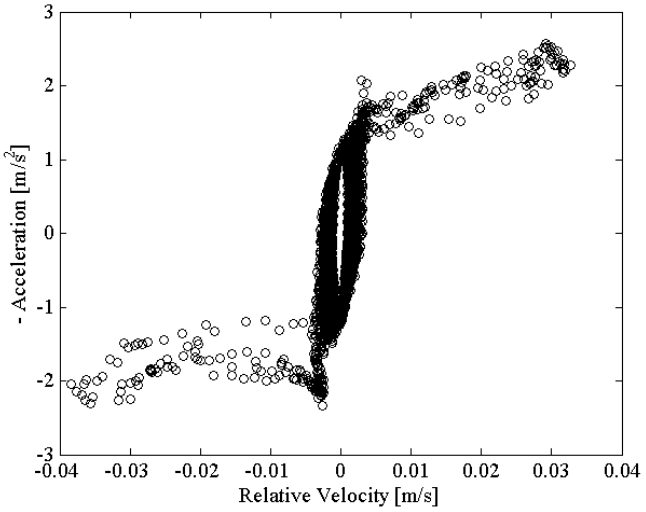

(j) 76.6N

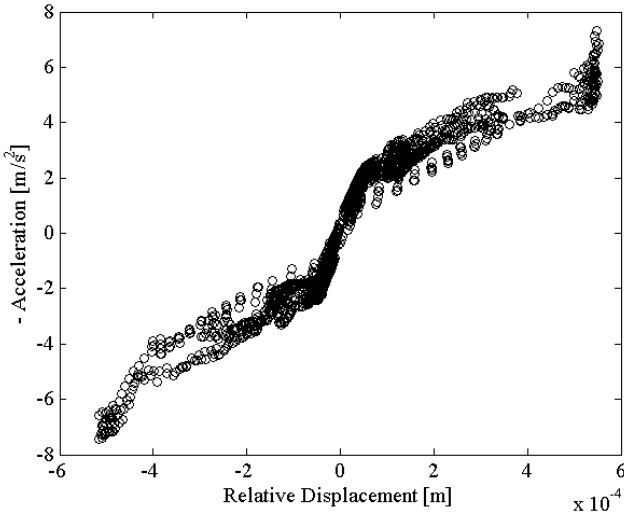

(k) 95.6N

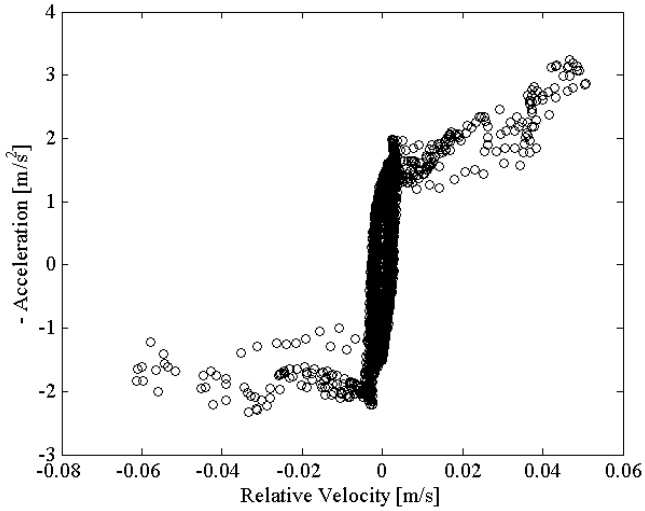

(l) 95.6N

Figure 11 (following): Qualitative stiffness (left) and damping (right) curves across the back wing-to-payload connection around the third mode computed using RFS method for 6 different levels of sine-sweep excitation

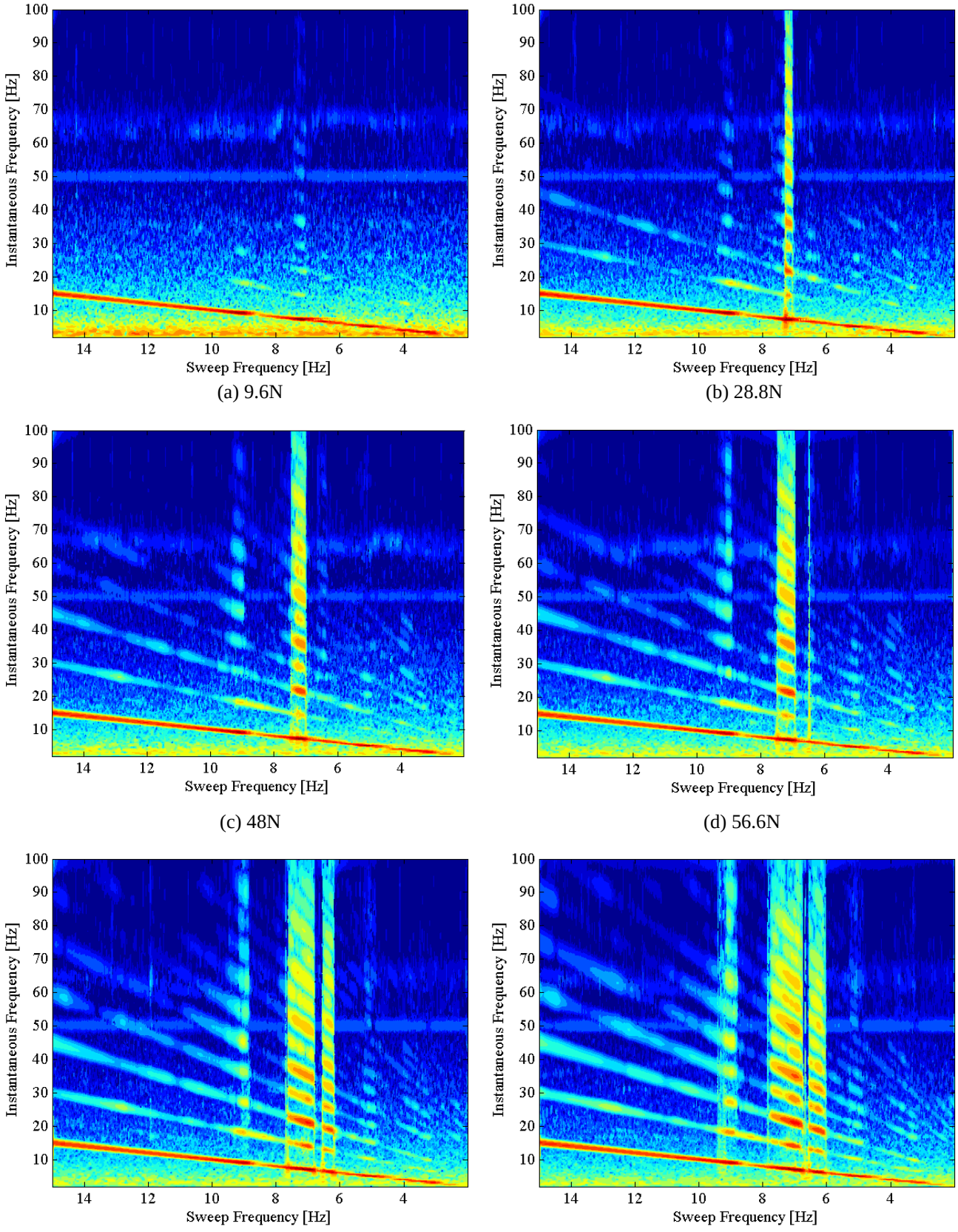

(a) 9.6N (b) 28.8N

(c) 48N (d) 56.6N

(e) 76.6N (f) 95.6N

Figure 12: Wavelet transform amplitudes (in logarithmic scaling) of the vertical acceleration measured at the back wing-to-payload connection, payload side for 6 different levels of sine-sweep excitation

Corresponding wavelet transforms amplitudes are plotted in Figure 12 and cover the whole excited frequency band. Low level response (a) mainly exhibits the fundamental and almost no harmonic components. Those ones begin appearing at 28.8N (b) and around the third mode at 7Hz. Both odd and even harmonics are present revealing and non-smooth nonlinearity behaviour although odd ones seem dominant. They keep growing with the excitation level and also tend to pop up on other modes (e), mainly the second and the fourth ones.

6 CONCLUSIONS

This paper showed how sine-sweep measurements from a Ground Vibration Testing campaign can provide insightful information about the nonlinear behaviour of a large-scale aircraft structures. A better understanding of the complex involved mechanisms is made possible by the use of two conceptually simple but powerful tools, namely the restoring force surface method and the wavelet transform-based time frequency analysis.

The demonstration of their efficiency and reliability was performed by exploiting a simple but representative finite-element model of an aircraft wing with a connected payload at its tip. The correct nonlinear behaviour in stiffness was properly retrieved and physical parameters such as the clearances were also well assessed.

Finally the investigation of the nonlinear dynamics of a full-scale F-16 aircraft possessing nonlinear wing-to-payload mounting interfaces was tackled. Sine-sweep data combined with the two described methods of nonlinear characterisation enabled to highlight the different nonlinear mechanisms occurring in the connection. Namely, coulomb friction, loosing of the assembly and impacts were retrieved by the computation of qualitative stiffness and damping curves.

ACKNOWLEDGMENTS

The authors T. Dossogne and J.P. Noël are Research Fellow (FRIA fellowship) and Postdoctoral Researcher, respectively, of the *Fonds de la Recherche Scientifique* – FNRS which is gratefully acknowledged.

7 REFERENCES

[1] European Commission. *European aeronautics: a vision for 2020*. Office for Official Publications of the European Communities, Luxembourg, 2001.

[2] C.M. Denegri Jr. Limit cycle oscillation flight test results of a fighter with external stores. *Journal of Aircraft*, 37(5):761–769, 2000.

[3] J.R. Ahlquist, J.M. Carreno, H. Climent, R. de Diego, and J. de Alba. Assessment of nonlinear structural response in A400M GVT. In *Proceedings of the 28th International Modal Analysis Conference (IMAC)*, Jacksonville, FL, 2010.

[4] K. Worden and G.R. Tomlinson. *Nonlinearity in Structural Dynamics: Detection, Identification and Modelling*. Institute of Physics Publishing, Bristol, UK, 2001.

[5] S.F. Masri and T.K. Caughey. A nonparametric identification technique for nonlinear dynamic problems. *Journal of Applied Mechanics*, 46:433–447, 1979.

[6] M.A. Al-Hadid and J.R. Wright. Application of the force-state mapping approach to the identification of non-linear systems. *Mechanical Systems and Signal Processing*, 4:463–482, 1990.

[7] K. Worden, D. Hickey, M. Haroon, and D.E. Adams. Nonlinear system identification of automotive dampers: A time and frequency-domain analysis. *Mechanical Systems and Signal Processing*, 23:104–126, 2009.

[8] G. Kerschen, J.C. Golinval, and K. Worden. Theoretical and experimental identification of a non-linear beam. *Journal of Sound and Vibration*, 244(4):597–613, 2001.

[9] W.J. Staszewski. Analysis of non-linear systems using wavelets. *Proceedings of the Institution of Mechanical Engineers Part C – Journal of Mechanical Engineering Science*, 214(11):1339–1353, 2000

[10] J. Lau, B. Peeters, J. Debille, Q. Guzek, W. Flynn, D.S. Lange and T. Kahlmann. Ground Vibration Testing Master Class: modern testing and analysis concepts applied to an F-16 aircraft, In *Proceedings of the International Modal Analysis Conference*, Jacksonville, FL, 2011.

[11] B. Peeters et al. Modern Solutions for Ground Vibration Testing of Large Aircraft. In *Proceedings of the 26th International Modal Analysis Conference (IMAC)*, Orlando, FL, 2008.

[12] J.P. Noël, L. Renson, G. Kerschen, B. Peeters, S. Manzato, and J. Debille. Nonlinear dynamic analysis of an F-16 aircraft using GVT data. In *Proceedings of the International Forum of Aeroelasticity and Structural Dynamic*, Bristol, 2013

[13] B. Peeters, H. Van der Auweraer, P. Guillaume, and J. Leuridan. The polymax frequency-domain method: a new standard for modal parameter estimation? *Shock and Vibration*, 11:395-409, 2004.

8 COPYRIGHT STATEMENT